# Probing the Nature of High-Redshift Long GRB 250114A and Its Magnetar Central Engine

Wen-Yuan Yu, Hou-Jun Lü, 1, Xiao Tian, Liang-Jun Chen, And En-Wei Liang

<sup>1</sup> Guangxi Key Laboratory for Relativistic Astrophysics, School of Physical Science and Technology, Guangxi University, Nanning 530004, China

## ABSTRACT

GRB 250114A is a long-duration gamma-ray burst (GRB) which triggered the Swift/BAT with a spectroscopic high-redshift at z=4.732. The light curve of the prompt emission is composed of three distinct emission episodes, which are separated by quiescent gaps ranging from tens to hundreds of seconds. While the X-ray light curve exhibits the canonical X-ray emission which is composed of several power-law segments superposition of a giant X-ray flare. More interestingly, there is still significant X-ray emission during the quiescent time in the prompt emission, suggesting a continuously active central engine whose power fluctuates across the  $\gamma$ -ray detectability threshold. In this paper, we propose a magnetar as the central engine of GRB 250114A by fitting the X-ray light curve, and infer a magnetic field strength  $B_{\rm p}=13.24^{+1.73}_{-5.84}\times10^{15}~{\rm G}$  and an initial spin period  $P_0=14.31^{+0.93}_{-3.16}~{\rm ms}$  of magnetar, with a jet correction, fall within a reasonable range. Furthermore, we also compare the prompt emission, X-ray afterglow,  $E_{\rm p}$ - $E_{\gamma,\rm iso}$ , and  $\varepsilon$ -distribution of GBR 250114A with those of other high-z sample-GRBs, and find no significant statistical differences between them.

## Keywords: Gamma-ray burst: general

# 1. INTRODUCTION

Gamma-ray bursts (GRBs) are the most violent and energetic explosions in the universe. Phenomenologically, they are generally classified into two types (e.g., long and short) with a division line at the observed duration  $T_{90} \sim 2$  s (Kouveliotou et al. 1993). The long GRBs are thought to be from the core-collapse of massive stars (Galama et al. 1998; Stanek et al. 2003; Malesani et al. 2004; Modjaz et al. 2006; Pian et al. 2006; Zhang 2006; Woosley & Bloom 2006; Cano et al. 2017; Lü et al. 2018a), while the short GRBs are proposed to be produced by mergers of two compact stellar objects (Barthelmy et al. 2005; Berger et al. 2005; Gehrels et al. 2005; Fox et al. 2005; Fong et al. 2010), such as neutron star-neutron star mergers (NS-NS; Paczynski 1986; Eichler et al. 1989), or neutron star-black hole mergers (NS-BH: Paczynski 1991).

Moreover, several peculiar GRBs, called short GRB with extended emission, are also claimed to originate from the merger of two compact stars, including GRB 060614 (Gehrels et al. 2006; Yang et al. 2015), GRB 211227A (Lü et al. 2022; Ferro et al. 2023), GRB 211211A (Rastinejad et al. 2022; Troja et al. 2022; Yang

et al. 2022; Chang et al. 2023; Liu et al. 2025), and GRB 230307A (Dichiara et al. 2023; Levan et al. 2024; Yang et al. 2024; Du et al. 2024; Sun et al. 2025). Recently, kilonova (KNe) emission has been observed in some of these sources, further supporting their compact binary merger origin (Zhang 2025; Liu et al. 2025). In addition, statistical studies suggest that such GRBs with extended emission have smaller plateau luminosities than the rest of the long GRB sample (Lenart et al. 2025), which makes the merger scenario more favorable. On the other hand, the coalescence systems are also the main targets as strong sources of gravitational wave (GW) events (Berger 2014). Especially, on 17 August 2017, the first direct detection of a GW event (GW170817) associated with short GRB 170817A was achieved by the Advanced Laser Interferometer Gravitational-wave Observatory (aLIGO) and Virgo (Abbott et al. 2017; Savchenko et al. 2017; Goldstein et al. 2017; Zhang et al. 2018), and it has confirmed that at least some short GRBs are indeed originate from the merger of compact stars. On the other hand, the detection of both GW170817 and GRB 170817A also opened a new window into studying such a catastrophic event across multiple messengers.

Historically, the first measured redshift for GRB 970508 was z = 0.835, which confirmd the cosmolog-

<sup>\*</sup> Corresponding author (LHJ) email: lhj@gxu.edu.cn

ical origin of GRBs (Metzger et al. 1997). Over the past few decades, the redshift of an increasing number of GRBs have been measured with a range from z = 0.085 to z = 9.4 (Galama et al. 1998; Cucchiara et al. 2011). Especially, several high-redshift GRBs are reported, including GRB 080913 at z = 6.7 (Greiner et al. 2009), GRB 090423 at z = 8.2 (Tanvir et al. 2009; Salvaterra et al. 2009), and the most distant candidate with a photometric redshift at z = 9.4 for GRB 090429B (Cucchiara et al. 2011). On the one hand, the highredshift of these GRBs has challenged the classification of GRBs (Zhang et al. 2009). If this is the case, the multiple observational criteria (Zhang et al. 2009), a new classification of GRBs (Lü et al. 2010) and the threedimensional of GRB prompt emission (Lü et al. 2014) have been proposed to study the GRB classification. On the other hand, even though the redshifts of hundreds of GRBs have now been measured, the distribution of these measurements remains heavily weighted towards low-z events, and the high-z GRBs are rare and exceptionally valuable. It has been established that high-zGRBs can be utilized to trace the cosmic star formation rate (Kistler et al. 2009; Ishida et al. 2011; Robertson & Ellis 2012). This enables the precise identification of high-redshift galaxies, facilitating the exploration of their metal and dust content (Tanvir et al. 2009; Salvaterra et al. 2013). Furthermore, they can be used to place limits on the mass of dark matter particles (de Souza et al. 2013) and on the degree of primordial density non-Gaussianity (Maio et al. 2012), as well as to gauge the intensity of the local intergalactic radiation field (Inoue et al. 2010). Additionally, the high-z GRBs can be employed to constrain fourth-order cosmographic expansions at (z > 1) (Hu & Wang 2022), and provide direct and/or indirect evidence of the first massive, metal-free stars, also known as Population III stars (Wang et al. 2012; Ma et al. 2015).

From an observational point of view, the prompt emission of a subset of long GRBs is composed of multiple emission episodes with quiescent times of up to hundreds of seconds, as detected by both the Fermi/Gamma-ray Burst Monitor (GBM) and the Swift/Burst Alert Telescope (BAT; Koshut et al. 1995; Lazzati 2005; Bernardini et al. 2013; Hu et al. 2014; Lan et al. 2018). Lan et al. (2018) found that certain Fermi/GBM-detected GRBs show multiple emission phases with quiescent intervals, yet the two episodes do not exhibit significant differences in their peak energies  $(E_{\rm p})$ . Similarly, Hu et al. (2014) reported that some GRBs observed by Swift display multi-stage radiation characteristics. These findings raise important questions: Do these emission episodes originate from different physical processes?

Or are they simply manifestations of reactivities of the central engine, with the high-energy component being absent during one of the episodes and only low-energy emission persisting?

Recently, a high-redshift GRB 250114A was detected by Swift/BAT with a redshift of z = 4.732 (Klingler et al. 2025; Malesani et al. 2025). The prompt emission of GRB 250114A consists of a triple-episode structure with two long-duration gaps which are quite similar to those observed precursors by the Burst And Transient Source Experiment (BATSE) (Koshut et al. 1995) and the Fermi/GBM (Lan et al. 2018; Coppin et al. 2020), while the X-ray afterglow light curve exhibits a flare phase and a plateau emission. More interestingly, significant X-ray emission was observed during the quiescent time in the prompt emission. Based on the properties of its multiwavelength data presented here, the central engine of GRB 250114A appears to be a magnetar. We present our data reduction and temporal-spectral analyses of data for GRB 250114 in Section 2. In Section 3, we compare the prompt emission and X-ray afterglow of GRB 250114A with those of other high-z (e.g., z > 4.5) GRBs. The magnetar-engine fitting procedure and a discussion of the physical implications are presented in Section 4. Conclusions and discussion are drawn in Section 5 and Section 6, respectively. Throughout the paper, we adopt a concordance cosmology with  $\Omega_M = 0.30$ ,  $\Omega_{\Lambda} = 0.70$ , and  $H_0 = 70 \,\mathrm{km \, s^{-1} \, Mpc^{-1}}$ .

# 2. DATA REDUCTION AND ANALYSIS

# 2.1. Swift/BAT Observations

GRB 250114A initially triggered the Swift/BAT on 14 January 2025 at 07:33:19 UT (Klingler et al. 2025). We downloaded the BAT data from the Swift website<sup>1</sup>, and use the standard HEASOFT v6.34 to process the BAT data. The BAT light curve in 15–350 keV is extracted with fixed 1 s time-bin by using batbinevt and employing the standard mask-weighting technique. The background is extracted using two time intervals before and after the burst, and then model the background as Poisson noise which is the standard back ground model for prompt emission in BAT events. The duration of the prompt emission can be estimated as  $T_{90,\text{BAT}} = 294 \pm 13 \text{ s in the } 15\text{-}350 \text{ keV}$ . Temporal structure analysis via the Bayesian Blocks algorithm (Scargle 1998) can identify three distinct emission episodes (see Figure 1), named as episode-I, II and III, with the falsepositive probability threshold set to  $p_0 = 0.05$  by using

https://www.swift.ac.uk/swift\_portal/getobject.php?name= GRB+250114A

the astropy.stats.bayesian\_blocks implementation. The analysis was performed on the BAT light curve in the 15–350 keV energy band objectively to identify significant temporal changes in the count rate, which serves to define the boundaries of the emission episodes for subsequent temporal analysis.

We also extract the time-averaged spectrum of the prompt emission observed by BAT, and several spectral models can be selected to test the spectral fitting of the burst, such as power law (PL), cutoff power law (CPL), Band function (Band), and Blackbody (BB), as well as combinations of any two models. It is found that the CPL model is the best one to adequately describe the observed data by comparing the goodness of different model fits to invoke the Bayesian information criteria (BIC). One has photon index  $\Gamma = 0.34 \pm 0.63$ and  $E_{\rm p} = 51 \pm 6$  keV. Then, we also perform the timeresolved spectrum on each episode to present the spectral evolution. It is found that the episode-I includes two pulses, and the spectrum of each pulse can be fitted well by CPL model (see Table 1). One needs to note that there is still significant X-ray emission during episode-II, episode-III, and the quiescent time between them. By jointing to the BAT and X-ray emissions during episode-II and episode-III, we also find that the CPL model is the best one to fit the time-resolved spectra, the fitting results are shown in Figure 1 and Table 1.

## 2.2. Swift/XRT and Follow-up Observations

The Swift X-Ray Telescope (XRT) began observing the field at 117 s after the BAT trigger (Dichiara et al. 2025), and an optical counterpart was discovered by the Ultraviolet/Optical Telescope (UVOT; Klingler et al. 2025). Subsequently, spectroscopic observations by the Very Large Telescope (VLT)/X-shooter derived a redshift for this GRB is z=4.732 (Malesani et al. 2025). Moreover, the optical afterglow follow-up observations are also reported by Gamma-ray Coordinates Network (GCN), and we collated the observed optical data from GCN reports, shown in the left panel of Figure 2 (An et al. 2025; Antier et al. 2025; Brivio et al. 2025; Ghosh et al. 2025; Malesani & Izzo 2025; Pérez-Fournon & Poidevin 2025).

We downloaded the XRT data of GRB 250114A from the Swift archive<sup>2</sup>. Figure 2 shows the X-ray light curve of GRB 250114A in the energy range of 0.3-10 keV. The X-ray light curve exhibits the canonical X-ray emission (Zhang 2006; Nousek et al. 2006) that seems to be composed of several power-law segments: an initial steep

decay smoothly connected with a plateau phase and followed by a normal decay segment, and a giant X-ray flare is superimposed on the steep decay segment. Then, we perform an empirical fitting to the X-ray light curve with a power-law + two smooth broken power-law models, it can be expressed as (Liang et al. 2007; Tian et al. 2025),

$$F_1 = F_{0,1} \left(\frac{t}{t_1}\right)^{-\alpha_1},\tag{1}$$

$$F_2 = F_{0,2} \left[ \left( \frac{t}{t_{\rm b,2}} \right)^{\omega_2 \alpha_2} + \left( \frac{t}{t_{\rm b,2}} \right)^{\omega_2 \alpha_3} \right]^{-1/\omega_2},$$
 (2)

$$F_3 = F_{0,3} \left[ \left( \frac{t}{t_{\text{b},3}} \right)^{\omega_3 \alpha_4} + \left( \frac{t}{t_{\text{b},3}} \right)^{\omega_3 \alpha_5} \right]^{-1/\omega_3}.$$
 (3)

The total X-ray light curve can be fitting by the superposition of those three components,

$$F = F_1 + F_2 + F_3. (4)$$

Here,  $t_1$  is the starting time of X-ray observations,  $t_{\rm b,2}$  and  $t_{\rm b,3}$  are the two break times for the flare and plateau emissions.  $\alpha_1$  is the initial power-law decay index,  $\alpha_2$  and  $\alpha_3$  are the rise and decay index before and after  $t_{\rm b,2}$ ,  $\alpha_4$  and  $\alpha_5$  are the decay index before and after  $t_{\rm b,3}$ .  $\omega_2$  and  $\omega_3$  describe the sharpness of the break at  $t_{\rm b,2}$  and  $t_{\rm b,3}$ , and fixed with  $\omega_2 = 10$  and  $\omega_3 = 7$ .

One can adopt a Markov Chain Monte Carlo (MCMC) method to fit the light curve by invoking above one power-law + two smooth broken power-law model. The first segment is a power-law decay with the temporal index  $\alpha_1 = 4.22^{+0.19}_{-0.18}$ , which is consistent with the tail emission of prompt  $\gamma$ -ray from curvature effect (Kumar & Panaitescu 2000; Liang et al. 2007; Uhm & Zhang 2015). The flare exhibits a fast rise phase followed by a rapid decay phase with the temporal index  $\alpha_2$  =  $-9.14 \pm 0.38$  and  $\alpha_3 = 7.52^{+0.15}_{-0.14}$ , and the break time is  $t_{\rm b,2} = 277.50^{+0.80}_{-0.78}$  s. In the plateau phase, the temporal decay index before and after the break time  $t_{\rm b,3}=$ 15860 $^{+2532}_{-2344}$  s are  $\alpha_4=0.53^{+0.02}_{-0.03}$  and  $\alpha_5=1.70^{+0.38}_{-0.28}$ , respectively. The peak fluxes at the break time of the flare and plateau are  $F_{\rm b,2} = (4.33 \pm 0.08) \times 10^{-9} {\rm erg} {\rm cm}^{-2}$  ${\rm s}^{-1}$  and  $F_{\rm b,3} = (2.48 \pm 0.30) \times 10^{-12} {\rm erg \ cm}^{-2} {\rm \ s}^{-1}$ , respectively. The fitting results of X-ray light curve for GRB 250114 are shown in Figure 2 and Table 2.

# 2.3. Overlapping between $\gamma$ -ray and X-ray emissions

More interestingly, it is found that the X-ray flare emission of GRB 250114A was simultaneously observed by BAT in episode- II and episode-III by comparing the light curves of X-ray and  $\gamma$ -ray. Then, we analyzed the joint spectral fit for the two emission episodes in the overlapping portion of the XRT and BAT data.

<sup>&</sup>lt;sup>2</sup> https://www.swift.ac.uk/xrt curves/01281241/

For the episode- II, the time-averaged spectrum from 112 s to 137 s is best fit by a cutoff power-law model with  $E_{\rm p}=55\pm16$  keV. For the episode-III, we temporally sliced it into four slices based on the shape of the light curve, namely, (210-232) s, (232-253) s, (253-282) s, (282-320) s. All the time-averaged spectral of those slices are best fit by a cutoff power-law model, and the values of  $E_{\rm p}$  are presented in the Table 1<sup>3</sup> It is found that the spectral evolution is from soft to hard in episode-III.

On the other hand, there is a quiescent period between episode- II and episode-III in the prompt emission, but the so-called quiescent period is not completely quiet as seen in the X-ray light curve from XRT (Figure 1). It is notable that there is still significant X-ray emission during the quiescent period, suggesting that the central engine may be still active, with this phase lasting hundreds of seconds.

# 3. COMPARISON WITH OTHER HIGH-REDSHIFT GRBS

Over the past few decades, Swift has detected hundreds of GRBs with measured redshifts, yet those at z > 4.5 remain a tiny minority. The rate of GRBs detected by Swift which end up to have their redshift measured with z > 4.5 is approximately 1.5 events per year. In order to compare the properties of prompt emission and X-ray afterglow of GRB 250114A and those of other high-z (e.g., z > 4.5) GRBs, we first select the sample-GRBs which are taken from (Liu et al. 2025), and then extract the light curves of both BAT and XRT. Figure 3 shows the prompt emission light curves of sample-GRBs and GRB 250114A in the rest frame. From a statistical perspective, the duration of GRB 250114A in the rest frame appears to be longer than that of other highz sample-GRBs. Moreover, we also plot the X-ray afterglow of GRB 250114A together with those of high-z sample-GRBs in the rest frame, we find that no statistically significant difference between them.

On the other hand, Amati et al. (2002) discovered that a majority of long-duration GRBs exhibit a positive correlation between the peak energy  $(E_{\rm p})$  and the isotropic burst energy  $(E_{\gamma,\rm iso})$ , namely,  $E_{\mathfrak p} \propto E_{\gamma,\rm iso}^{1/2}$ , even the dispersion of the correlation is large, and outliers do exist (Zhang et al. 2009). However, the Amati relation of the majority of short-duration GRBs appears to be a slightly shallower in terms of power index when compared with that of long GRBs (Zhang et al. 2009). Lü et al. (2010) proposed a new phenomenological classifi-

cation method for GRBs by adopting a new parameter  $\varepsilon = E_{\gamma, \text{iso}, 52}/E_{\text{p,z,2}}^{5/3}$ , which has proven to be highly effective in the classification of high-z GRBs. Here,  $E_{\gamma, \text{iso}, 52}$  is the isotropic gamma-ray energy in units of  $10^{52}$  erg, and  $E_{\text{p,z,2}}$  is the cosmic rest-frame spectral peak energy in units of 100 keV. They found that the  $\varepsilon$  has a clear bimodal distribution (high- and low-  $\varepsilon$  regions) with a division line at  $\varepsilon \sim 0.03$ , and the low- and high- $\varepsilon$  regions corresponding to the mergers of two compact stars (type I) and the death of massive stars (type II), respectively.

By calculating the isotropic burst energy via k-correction (Bloom et al. 2001), one has  $E_{\gamma,\rm iso}=(1.7\pm0.2)\times10^{53}\,\rm erg$  for GRB 250114A. Due to the lack of enough optical afterglow data, it is difficult to directly constrain the jet opening angle for GRB 250114A. Alternatively, we adopt the empirical Ghirlanda relation which presented the relationship between the jet opening angle, the isotropic gamma-ray energy, and the peak energy of the burst spectrum (Goldstein et al. 2016) to estimate the opening angle. If this is the case, one can roughly derive a jet opening angle as  $\theta_{\rm j}=3.14^{\circ}$  (corresponding to a beaming factor  $f_{\rm b}=1-\cos(\theta_{\rm j})\sim0.0015$ ), and the jet corrected energy is about  $E_{\gamma}\sim2.55\times10^{50}\,\rm erg$ .

Figure 5(a) shows the  $E_{\rm p} - E_{\gamma,\rm iso}$  correlation for GRB 250114A and other long-duration GRBs. It is found that GRB 250114A falls squarely on the main sequence of long-duration GRBs, thereby suggesting the potential for a shared progenitor with that of other long-duration GRBs. Adopting the method from Lü et al. (2010), one can calculate  $\varepsilon \sim 2.84$ , which is located in the high- $\varepsilon$ region. The high- $\varepsilon$  value of GRB 250114A suggests that its progenitor is consistent with Type II population from the death of massive stars (see Figure 5). Furthermore, wo also plot the high-z GRBs in the  $E_{\rm p}-E_{\gamma,\rm iso}$  and  $\varepsilon$ -distribution diagrams to facilitate a comparison with GRB 250114A, as illustrated in Figure 5. It has been established that the location of most high-z GRBs is situated within into the main sequence for long-duration GRBs in the  $E_p - E_{\gamma,iso}$  diagram and the high- $\varepsilon$  region.

On the other hand, the  $E_{\rm p}-E_{\gamma,\rm iso}$  diagram is not fool-proof method to identify the progenitors (Kang et al. 2025). Alternatively, another well-established empirical correlation is so-called Dainotti relation (Dainotti et al. 2013; Rowlinson et al. 2014) which is used to judge the origin of core-collapse for GRBs. This relation reveals an anti-correlation between the duration of X-ray plateau in rest-frame ( $T_a^*$ ) and the X-ray plateau luminosity ( $L_X$ ) of GRBs, which has been confirmed in large samples of long-duration bursts and proposed as a potential tool for GRB standardization (Lenart et al. 2025). For GRB 250114A, one can obtain  $T_a^* = (2.76^{+0.40}_{-0.40}) \times 10^3$  s

<sup>&</sup>lt;sup>3</sup> One needs to note that the spectral fitting results of time intervals (112–137)s, (210–232)s, and (253–282)s are derived from joint XRT+BAT+optical (see Fu et al. 2024.)

and  $L_X = (5.63^{+0.69}_{-0.62}) \times 10^{47} \text{ erg s}^{-1} \text{ from our XRT afterglow fits, and it is found that it is also located within the core-collapse (Type II) region.$ 

## 4. PHYSICAL INTERPRETATION

The long-duration prompt emission of GRB 250114A suggests that the progenitor is likely related to the collapse of a massive star. In the collapsar scenario, a hyper-accreting black hole or a rapidly spinning magnetar may be formed as the central engine (Usov 1992; Dai & Lu 1998; Zhang & Mészáros 2001; Lei et al. 2013; Liu et al. 2017). It is imperative that the engine remains operational for a sufficient duration to ensure the jet head successfully breaks out of the star and produces a successful jet. Based on the feature of X-ray afterglow emission of GRB 250114A, a magnetar with a high surface magnetic field and a short-period is proposed to be a central engine of GRB 250114A. It is evident that the observed X-ray plateau emission is attributable to magnetic dipole radiation from the newborn millisecond magnetar prior to its collapse (Dai & Lu 1998; Zhang & Mészáros 2001; Metzger et al. 2011; Lü & Zhang 2014).

The total rotational energy of the newborn millisecond magnetar can be expressed as (Zhang & Mészáros 2001; Lü et al. 2018b):

$$E_{\rm rot} = \frac{1}{2}I\Omega^2 \approx 2 \times 10^{52} \,\mathrm{erg} \,M_{1.4}R_6^2 P_{0,-3}^{-2},$$
 (5)

where I is the moment of inertia,  $\Omega$  is the angular frequency,  $P_{0,-3}$  is the initial period of the neutron star in units of milliseconds,  $R_6$  is the radius of the neutron star in units of  $10^6$  cm,  $M_{1.4} = 1.4 M_{\odot}$  is the mass of neutron star. By considering a newly born magnetar, it is spun down via electromagnetic (EM) dipole radiation,

$$-\frac{dE_{\rm rot}}{dt} = -I\Omega\dot{\Omega} = L_{\rm EM} = \frac{B_{\rm p}^2 R^6 \Omega^4}{6c^3},\tag{6}$$

$$L_{\rm EM}(t) = L_0(1 + \frac{t}{\tau})^{-2}.$$
 (7)

Here,  $B_{\rm p}$  is surface magnetic filed, c is speed of light,  $L_0$  and  $\tau$  are the initial kinetic luminosity and the characteristic spin-down timescales, respectively, namely,

$$L_0 = 1.0 \times 10^{49} \text{ erg s}^{-1} (B_{p,15}^2 P_{0,-3}^{-4} R_6^6),$$
 (8)

$$\tau = 2.05 \times 10^3 \text{ s} \left( I_{45} B_{\text{p},15}^{-2} P_{0,-3}^2 R_6^{-6} \right),$$
 (9)

where  $B_{\rm p,15}$  is the magnetic filed strength in units of  $10^{15}$  G, and  $I_{45}$  is the moment of inertia in units of  $10^{45}$  g cm<sup>2</sup>.

# 4.1. Model fitting with magnetar central engine

In this section, we invoke the with the full vacuum dipole magnetar (Zhang & Mészáros 2001; Rowlinson et al. 2013) central engine model to fit the flaresubtracted X-ray plateau emission<sup>4</sup> by adopting the open-source software package Redback (Sarin et al. 2024). Since such magnetar model is also employed in the context of numerous long-duration GRBs exhibiting X-ray plateau emission (Fan & Xu 2006; Troja et al. 2007; Lyons et al. 2010; Bernardini et al. 2012; Shan et al. 2024). Although recent work has explored the possible role of higher-order multipolar fields (e.g., quadrupole, octupole) in shaping the early-time lightcurve behavior (Wang et al. 2024), such effects require rather extreme initial configurations. Based on the fitting results, the plateau luminosity of GRB 250114A is about  $2 \times 10^{48}$  erg/s which is consistent with the numerical calculation with dipole radiation dominated (Wang et al. 2024). On the other hand, the decay slope after the plateau is steeper than that predicted from the higher-order field components. So that, we only consider the dipole radiation of magnetar in this work to do the model fitting.

In the magnetar framework, the total luminosity is modeled as the sum of a dipole spin-down component and an underlying power-law decay,

$$L(t) = L_0 \left( 1 + \frac{t}{\tau} \right)^{\frac{1+n}{1-n}} + A_1 t^{-\alpha_1}, \qquad (10)$$

where n is the braking index of magnetar (Lasky et al. 2017). The extra power-law term with amplitude  $A_1$  and index  $\alpha_1$  accounts for the high-latitude (curvature) emission of the prompt phase (Kumar & Panaitescu 2000). The time of the observer frame is converted to t/(1+z) in the source frame, and the bolometric luminosity L(t) in the above equation is derived from the observed X-ray flux of plateau  $F_{\rm obs}$  directly into an isotropic bolometric luminosity,

$$L(t) = 4\pi D_L^2 F_{\text{obs}},\tag{11}$$

where  $D_L$  is the luminosity distance.

There are five free parameters (i.e.,  $L_0$ ,  $\tau$ , n,  $A_1$  and  $\alpha_1$ ) by invoking the full vacuum dipole magnetar model. The prior distributions for the parameters were

<sup>&</sup>lt;sup>4</sup> We excluded X-ray flare emission which is believed to be from central engine re-activity in our model fitting.

defined as follows:

$$\begin{cases} A_1 \sim \text{LogUniform} (10^{-20}, 10^{20}), \\ \alpha_1 \sim \text{Uniform} (-10, -0.5), \\ L_0 \sim \text{LogUniform} (10^{30}, 10^{55}) \text{ erg s}^{-1}, \\ \tau \sim \text{LogUniform} (10^2, 10^6) \text{ s}, \\ n \sim \text{Uniform} (1, 7). \end{cases}$$

To sample the posterior distributions, we employ the dynesty sampler (Speagle 2020), a pure Python, MIT-licensed dynamic nested sampling package for estimating Bayesian posteriors and evidences. We configure dynesty with nlive=1000 live points and use the sample='rslice' method. The rslice option implements random-direction slice sampling: at each iteration, a random direction in the parameter space is chosen and a one-dimensional slice sampling step is performed along that direction, which improves mixing and exploration efficiency in multi-dimensional posteriors.

# 4.2. Fitting Results and inferred Magnetar Parameters

Figure 6 shows the fitting results by using the magnetar model in the rest-frame to the XRT light curve with flare-subtracted of GRB 250114A. The 2D histograms and parameter constraints of the model fit by invoking the dynesty sampler are shown in Figure 6, and the values of the parameter constraints are reported in the Table 3. It is found that four free parameters (i.e.,  $L_0$ , n,  $A_1$  and  $\alpha_1$ ), can be constrained very well. Based on the results of best-fit for the spin-down luminosity  $L_0 = 2.78^{+0.46}_{-0.42} \times 10^{48}\,\mathrm{erg\,s^{-1}}$  and characteristic timescale  $\tau = 2397^{+1057}_{-310}$  s, one can directly infer the surface polar cap magnetic field strength  $B_\mathrm{p}$  and initial spin period  $P_0$  of the magnetar by adopting Eqs. (8) and (9).

It is worth noting that a gap in the X-ray light curve between  $t \sim 2 \times 10^2 \,\mathrm{s}$  and  $t \sim 8 \times 10^2 \,\mathrm{s}$  in the rest frame should be a potential systematic uncertainty in the identification of the magnetar spin-down plateau. In particular, the emission at  $t \sim 10^2$  s is possible to be contributed from both tail emission of the X-ray flare and spin-down of magnetar. In order to confirm the validity of this hypothesis, the fits were repeated using data exclusively from  $t \ge 8 \times 10^2$  s (i.e., excluding the flare and power-law components). It is found that the spin-down timescale and the braking index n become poorly constrained with larger uncertainties. Therefore, although we believe the possibility that flare contamination may affect the earliest post-gap points, the flare-subtracted fit provides the most robust and tightly constrained interpretation of the available data.

By adopting the derived a jet opening angle of  $\theta_{\rm j}=3.14^{\circ}$  from Goldstein et al. 2016 and assuming a radiation efficiency  $\eta\sim0.1$ , one can estimate the magnetar

initial spin period and polar magnetic field strength to be  $P_0 = 14.31^{+0.93}_{-3.16} \,\mathrm{ms}$  and  $B_\mathrm{p} = 13.24^{+1.73}_{-5.84} \times 10^{15} \,\mathrm{G}$ , respectively. Moreover, by comparing the inferred  $B_\mathrm{p}$  and  $P_0$  of GRB 250114A with that of other magnetar candidates GRBs taken from Lü & Zhang (2014), we find that the derived values of those parameters fall into the reasonable range (see Figure 7).

Moreover, the early peak of optical emission is likely to be associated with the prompt emission of GRB itself, as shown in Figure 2. While the lack of enough optical observations at late time seems to be a peak or a plateau emission which is consistent with X-ray emission, but it is difficult to confirm due to the few optical observations.

# 5. CONCLUSIONS

GRB 250114A is a long-duration GRB that triggered Swift/BAT (Klingler et al. 2025), and the spectroscopic observations by the Very Large Telescope derived a redshift at z = 4.732 (Malesani et al. 2025). The prompt emission of GRB 250114A shows three distinct emission episodes which are identified via the Bayesian Blocks algorithm (Scargle 1998). The X-ray light curve displays the canonical X-ray emission that appears to be composed of multiple power-law segments: an initial steep decay smoothly connected with a plateau phase and followed by a normal decay segment, and a giant X-ray flare is superimposed on the steep decay segment. More interestingly, it is found that the X-ray flare emission of GRB 250114A was simultaneously observed by BAT in episode-II and episode-III by comparing the light curves of X-ray and  $\gamma$ -ray. There is still significant X-ray emission during the quiescent period between the episode-II and episode-III.

By calculating the isotropic burst energy and extracting the spectra of GRB 250114A, one has  $E_{\gamma,iso}$  =  $(1.7\pm0.2)\times10^{53}$  erg and  $E_p = 51\pm6$  keV. GRB 250114A is located at the main sequence of long-duration GRBs in the  $E_{\rm p} - E_{\gamma,\rm iso}$  diagram, and is consistent with that of other long GRBs in high- $\varepsilon$  region. It suggests that GRB 250114A is possible shared a similar progenitor from the death of massive stars with that of other long-duration GRBs. Moreover, by comparing both prompt emission and X-ray afterglow with that of other high-z GRBs, it is found that the duration of GRB 250114A seems to be longer than that of other high-z sample-GRBs, but the peak flux of pulse of GRB 250114A is mixing with that of other high-z sample-GRBs. The X-ray afterglow appears to demonstrate no statistically significant difference between between them. In the  $E_{\rm p}-E_{\gamma,\rm iso}$  diagram and  $\varepsilon$ -distribution, the location of most high-z GRBs fall into the main sequence for long-duration GRBs in  $E_{\rm p}-E_{\gamma,\rm iso}$  and high- $\varepsilon$  region, respectively. Moreover, we find that GRB 250114A is also located within the corecollapse (Type II) region of Dainotti relation (Dainotti et al. 2010, 2011, 2013; Rowlinson et al. 2014), and the plateau luminosity-duration anti-correlation is also confirmed by other researchers in the literature (Stratta et al. 2018).

Based on the feature of X-ray afterglow emission of GRB 250114A, we propose a magnetar as a central engine of GRB 250114A. The observed X-ray plateau emission is hypothesised to be attributable to magnetic dipole radiation from the newborn millisecond magnetar prior to its collapse. Therefore, we model the X-ray plateau using the full vacuum dipole magnetar scenario implemented in Redback and sampled with dynesty. The magnetar central engine model provides well fit to the flare-subtracted light curve, yielding wellconstrained posterior distributions for  $L_0, \tau, n, A_1$ , and  $\alpha_1$ . If this is the case, we also infer the magnetic field strength  $B_{\rm p}=13.24^{+1.73}_{-5.84}\times 10^{15}~{\rm G}$  and initial spin period  $P_0=14.31^{+0.93}_{-3.16}$  ms with a jet correction, and it also falls into the reasonable range by comparing other candidates of magnetar central engine in long-duration GRBs.

Within the magnetar central engine scenario, the quiescence period (e.g., three episodes emission) in the prompt phase is possibly caused by accretor-propeller behaviour of the magnetar which is proposed by Bernardini et al. 2013. The  $\gamma$ -ray emission of episodes I and II are likely powered by active accretion onto the newborn magnetar, and the magnetic field rises rapidly and temporarily repels the infalling material. Therefore, the electromagnetic emission temporarily fades. The subsequent quiescent period in  $\gamma$ -ray, accompanied by significant X-ray emission, could mark a transition from accretor-propeller to the propeller regime. During this phase, the rapidly spinning magnetar's intense magnetic field effectively repels the infalling material, halting efficient accretion onto the surface and thus quenching the high-energy  $\gamma$ -ray production. However, the central engine remains active, the rotational energy of the magnetar can be dissipated through magnetic braking or interactions with the halted material, giving rise to the observed lower-energy X-ray emission. The eventual restart of intense  $\gamma$ -ray emission in episode-III would then correspond to the central engine overcoming this barrier and resuming active accretion. The observed evolution of the spectral peak energy  $E_p$  is also consistent with this picture of intermittent energy injection from a magnetar.

If the magnetar is indeed operating as the central engine in GRB 250114A, one question is that whether the total energy observed from GRB 250114A satisfies the energy budget of the newborn magnetar. The plateau energy can be calculated as  $E_{\rm X,iso} \sim L_x \times T_a^* \sim$  $1.56 \times 10^{51}$  erg, and the kinetic energy can be roughly estimated as  $E_{\rm K,iso} \sim 2.4 \times 10^{54}$  erg by adopting the method in Zhang et al. 2007 and Li et al. 2018. We find that the total energy of magnetar is larger than that sum of  $\gamma$ -ray energy, plateau energy, and kinetic energy after jet correction, namely,  $E_{\text{tot}} > (E_{\gamma,\text{iso}} + E_{X,\text{iso}} + E_{K,\text{iso}}) f_{\text{b}}$ . It suggests that at least the energy budget of magnetar central engine satisfies with output energy of observations. Excepting magnetar central engine model, the black hole central engine as a candidate to interpret GRB 250114A can not be ruled out. For example, fallback accretion onto a black hole (Kumar et al. 2008; Cannizzo & Gehrels 2009; Cannizzo et al. 2011; Lei et al. 2017; Lenart et al. 2025), or continued central engine activity from the hydrodynamical interactions of a single blast shock wave with the circumburst medium (e.g., Duffell & Ho 2020; Dereli-Bégué et al. 2022).

Moreover, the physical explanation of GRB 250114A that we adopt may not be the only one to the observations, and several physical models have also been invoked to interpret the observed X-ray flare, plateau emission, as well as the multi-episode prompt emission. For example, Dai et al. (2006) propose that the differential rotation of millisecond pulsar winds up internal poloidal fields into strong toroidal fields that buoyantly break through the surface and reconnect explosively, powering the X-ray flare. Nakar & Piran (2017) have shown that when the GRB jet breaks out of the star it inflates a cocoon whose expansion and interaction with the external medium can power wide-angle X-ray flares, with their luminosity and duration set by the cocoon's energy deposition and the degree of jet-stellar mixing. Perna et al. (2006) and Dall'Osso et al. (2017) also proposed that fragmentation in the accretion disk can reproduce the empirical statistical properties of the X-ray flares. Gao et al. (2023) propose a jet precession model to interpret the repeating emission episodes. Wang & Mészáros (2007) proposed the jet bow shock and relativistic jet itself to explain the two-episode emission.

Furthermore, other possible interpretations are also proposed, such as fallback accretion on the magnetar (Yu et al. 2024), or the magnetic barrier around the accretor (Proga & Zhang 2006), or the gravitational lensing (Paynter et al. 2021; Yang et al. 2021). However, more or less, each model above cannot fully interpret all properties of the observations of GRB 250114A from the light curve, spectrum, as well as the quiescent time.

The magnetar model currently presents the most selfconsistent framework for simultaneously explaining the sustained activity across energy bands and the specific temporal evolution observed in this event.

One is needed to note that the connection between long GRBs and the cosmic star formation rate (SFR) remains debated. Although some studies suggest that long GRBs broadly trace the SFR (Vergani et al. 2015), other works have reported deviations (Schneider et al. 2022; Dong et al. 2023). These discrepancies may in part be explained by the existence of a distinct population of low-luminosity GRBs (Virgili et al. 2009), or by possible contamination of the long-GRB sample by long-duration compact binary mergers (Petrosian & Dainotti 2024). More recent analyses also indicate that the GRB-SFR relation may be more complex than previously assumed, requiring consideration of multiple populations and evolutionary effects (Atteia et al. 2018; Arcier & Atteia 2022; Matsumoto et al. 2024).

On the other hand, the nature of the significant X-ray emission during the quiescent period remains in debate. Although most studies shown that the interval between pulses of prompt emission is a true "quiescent period". It indicates that the central engine switches off

during such quiescent period, subsequently re-initiating to power the sub-bursts of gamma-ray emission and X-ray flares in the afterglow. However, at least for GRB 250114A, it is found that the central engine never truly shuts down; rather, it persists in its activity. Just because of the  $\gtrsim 10\,\mathrm{keV}$   $\gamma$ -rays emission are absence, but is replaced by lower-energy X-ray emission. In summary, the central engine of GRB 250114A has been in operation to power those three-episode emissions and X-ray flare, even during the quiescent period in  $\gamma$ -rays emission.

# 7. ACKNOWLEDGMENTS

We acknowledge the use of the public data from the Swift/BAT and XRT Science Data Center. This work is supported by the Natural Science Foundation of China (grant Nos. 12494574, 11922301, and 12133003), the Natural Science Foundation of Guangxi (grant Nos. 2023GXNSFDA026007 and 2025FNFN99005), the Program of Bagui Scholars Program (LHJ), and the Guangxi Talent Program (Highland of Innovation Talents).

#### REFERENCES

Abbott, B. P., Abbott, R., Abbott, T. D., et al. 2017,PhRvL, 119, 16, 161101.doi:10.1103/PhysRevLett.119.161101

Amati, L., Frontera, F., Tavani, M., et al. 2002, A&A, 390, 81. doi:10.1051/0004-6361:20020722

An, J., Tinyanont, S., Anutarawiramkul, R., et al. 2025, GCN, 38929, 1.

Antier, S., Klotz, A., Akl, D., et al. 2025, GCN, 38946, 1.

Arcier, B. & Atteia, J.-L. 2022, ApJ, 933, 1, 17. doi:10.3847/1538-4357/ac6604

Atteia, J.-L., Dezalay, J.-P., Godet, O., et al. 2018, A&A, 610, A58. doi:10.1051/0004-6361/201731875

Barthelmy, S. D., Chincarini, G., Burrows, D. N., et al. 2005, Nature, 438, 7070, 994. doi:10.1038/nature04392

Berger, E., Price, P. A., Cenko, S. B., et al. 2005, Nature, 438, 7070, 988. doi:10.1038/nature04238

Berger, E. 2014, ARA&A, 52, 43. doi:10.1146/annurev-astro-081913-035926

Bernardini, M. G., Margutti, R., Mao, J., et al. 2012, A&A, 539, A3. doi:10.1051/0004-6361/201117895

Bernardini, M. G., Campana, S., Ghisellini, G., et al. 2013, ApJ, 775, 1, 67. doi:10.1088/0004-637X/775/1/67

Bloom, J. S., Frail, D. A., & Sari, R. 2001, AJ, 121, 6, 2879. doi:10.1086/321093

Brivio, R., D'Avanzo, P., Ferro, M., et al. 2025, GCN, 38933, 1.

Cannizzo, J. K. & Gehrels, N. 2009, ApJ, 700, 2, 1047. doi:10.1088/0004-637X/700/2/1047

Cannizzo, J. K., Troja, E., & Gehrels, N. 2011, ApJ, 734, 1, 35. doi:10.1088/0004-637X/734/1/35

Cano, Z., Wang, S.-Q., Dai, Z.-G., et al. 2017, Advances in Astronomy, 2017, 8929054. doi:10.1155/2017/8929054

Chang, X.-Z., Lü, H.-J., Yang, X., et al. 2023, ApJ, 943, 2, 146. doi:10.3847/1538-4357/aca969

Coppin, P., de Vries, K. D., & van Eijndhoven, N. 2020, PhRvD, 102, 10, 103014. doi:10.1103/PhysRevD.102.103014

Cucchiara, A., Levan, A. J., Fox, D. B., et al. 2011, ApJ, 736, 1, 7. doi:10.1088/0004-637X/736/1/7

Dai, Z. G., Wang, X. Y., Wu, X. F., et al. 2006, Science, 311, 5764, 1127. doi:10.1126/science.1123606

Dai, Z. G. & Lu, T. 1998, PhRvL, 81, 20, 4301. doi:10.1103/PhysRevLett.81.4301

Dainotti, M. G., Willingale, R., Capozziello, S., et al. 2010, ApJL, 722, 2, L215. doi:10.1088/2041-8205/722/2/L215

Dainotti, M. G., Ostrowski, M., & Willingale, R. 2011, MNRAS, 418, 4, 2202.

doi:10.1111/j.1365-2966.2011.19433.x

- Dainotti, M. G., Cardone, V. F., Piedipalumbo, E., et al. 2013, MNRAS, 436, 1, 82. doi:10.1093/mnras/stt1516
- Dall'Osso, S., Perna, R., Tanaka, T. L., et al. 2017, MNRAS, 464, 4, 4399. doi:10.1093/mnras/stw2695
- Dereli-Bégué, H., Pe'er, A., Ryde, F., et al. 2022, Nature Communications, 13, 5611. doi:10.1038/s41467-022-32881-1
- de Souza, R. S., Mesinger, A., Ferrara, A., et al. 2013, MNRAS, 432, 4, 3218. doi:10.1093/mnras/stt674
- Dichiara, S., Kennea, J. A., Page, K. L., et al. 2025, GCN, 38945, 1.
- Dichiara, S., Tsang, D., Troja, E., et al. 2023, ApJL, 954, 1, L29. doi:10.3847/2041-8213/acf21d
- Dong, X. F., Zhang, Z. B., Li, Q. M., et al. 2023, ApJ, 958, 1, 37. doi:10.3847/1538-4357/acf852
- Du, Z., Lü, H., Yuan, Y., et al. 2024, ApJL, 962, 2, L27. doi:10.3847/2041-8213/ad22e2
- Duffell, P. C. & Ho, A. Y. Q. 2020, ApJ, 900, 2, 193. doi:10.3847/1538-4357/aba90a
- Eichler, D., Livio, M., Piran, T., et al. 1989, Nature, 340, 6229, 126. doi:10.1038/340126a0
- Fan, Y.-Z. & Xu, D. 2006, MNRAS, 372, 1, L19. doi:10.1111/j.1745-3933.2006.00217.x
- Ferro, M., Brivio, R., D'Avanzo, P., et al. 2023, A&A, 678, A142. doi:10.1051/0004-6361/202347113
- Fong, W., Berger, E., & Fox, D. B. 2010, ApJ, 708, 1, 9. doi:10.1088/0004-637X/708/1/9
- Fox, D. B., Frail, D. A., Price, P. A., et al. 2005, Nature, 437, 7060, 845. doi:10.1038/nature04189
- Fu, S.-Y., Xu, D., Lei, W.-H., et al. 2024, ApJ, 977, 2, 197. doi:10.3847/1538-4357/ad8886
- Galama, T. J., Vreeswijk, P. M., van Paradijs, J., et al. 1998, Nature, 395, 6703, 670. doi:10.1038/27150
- Gao, H., Li, A., Lei, W.-H., et al. 2023, ApJ, 945, 1, 17. doi:10.3847/1538-4357/acba0d
- Gehrels, N., Sarazin, C. L., O'Brien, P. T., et al. 2005, Nature, 437, 7060, 851. doi:10.1038/nature04142
- Gehrels, N., Norris, J. P., Barthelmy, S. D., et al. 2006, Nature, 444, 7122, 1044. doi:10.1038/nature05376
- Ghosh, A., Razzaque, S., Moskvitin, A., et al. 2025, GCN, 38948, 1.
- Goldstein, A., Connaughton, V., Briggs, M. S., et al. 2016, ApJ, 818, 1, 18. doi:10.3847/0004-637X/818/1/18
- Goldstein, A., Veres, P., Burns, E., et al. 2017, ApJL, 848, 2, L14. doi:10.3847/2041-8213/aa8f41
- Greiner, J., Krühler, T., Fynbo, J. P. U., et al. 2009, ApJ, 693, 2, 1610. doi:10.1088/0004-637X/693/2/1610
- Hu, J. P. & Wang, F. Y. 2022, A&A, 661, A71. doi:10.1051/0004-6361/202142162

- Hu, Y.-D., Liang, E.-W., Xi, S.-Q., et al. 2014, ApJ, 789, 2, 145. doi:10.1088/0004-637X/789/2/145
- Inoue, S., Salvaterra, R., Choudhury, T. R., et al. 2010, MNRAS, 404, 4, 1938. doi:10.1111/j.1365-2966.2010.16414.x
- Ishida, E. E. O., de Souza, R. S., & Ferrara, A. 2011, MNRAS, 418, 1, 500. doi:10.1111/j.1365-2966.2011.19501.x
- Kang, Y., Zhu, J.-P., Yang, Y.-H., et al. 2025, A&A, 698, A250. doi:10.1051/0004-6361/202554448
- Kistler, M. D., Yüksel, H., Beacom, J. F., et al. 2009, ApJL, 705, 2, L104. doi:10.1088/0004-637X/705/2/L104
- Klingler, N. J., Brivio, R., DeLaunay, J. J., et al. 2025, GCN, 38927, 1.
- Koshut, T. M., Kouveliotou, C., Paciesas, W. S., et al. 1995, ApJ, 452, 145. doi:10.1086/176286
- Kouveliotou, C., Meegan, C. A., Fishman, G. J., et al. 1993, ApJL, 413, L101. doi:10.1086/186969
- Kumar, P. & Panaitescu, A. 2000, ApJL, 541, 2, L51. doi:10.1086/312905
- Kumar, P., Narayan, R., & Johnson, J. L. 2008, MNRAS, 388, 4, 1729. doi:10.1111/j.1365-2966.2008.13493.x
- Lan, L., Lü, H.-J., Zhong, S.-Q., et al. 2018, ApJ, 862, 2, 155. doi:10.3847/1538-4357/aacda6
- Lasky, P. D., Leris, C., Rowlinson, A., et al. 2017, ApJL, 843, 1, L1. doi:10.3847/2041-8213/aa79a7
- Lattimer, J. M. & Prakash, M. 2004, Science, 304, 5670, 536. doi:10.1126/science.1090720
- Lazzati, D. 2005, MNRAS, 357, 2, 722. doi:10.1111/j.1365-2966.2005.08687.x
- Lei, W.-H., Zhang, B., & Liang, E.-W. 2013, ApJ, 765, 2,  $125.\ doi:10.1088/0004-637X/765/2/125$
- Lei, W.-H., Zhang, B., Wu, X.-F., et al. 2017, ApJ, 849, 1, 47. doi:10.3847/1538-4357/aa9074
- Lenart, A. L., Dainotti, M. G., Khatiya, N., et al. 2025, Journal of High Energy Astrophysics, 47, 100384. doi:10.1016/j.jheap.2025.100384
- Levan, A. J., Gompertz, B. P., Salafia, O. S., et al. 2024, Nature, 626, 8000, 737. doi:10.1038/s41586-023-06759-1
- Li, L., Wu, X.-F., Lei, W.-H., et al. 2018, ApJS, 236, 2, 26. doi:10.3847/1538-4365/aabaf3
- Liang, E.-W., Zhang, B.-B., & Zhang, B. 2007, ApJ, 670, 1, 565. doi:10.1086/521870
- Liu, X.-X., Lü, H.-J., Chen, Q.-H., et al. 2025, ApJL, 988, 2, L46. doi:10.3847/2041-8213/adec83
- Liu, T., Gu, W.-M., & Zhang, B. 2017, NewAR, 79, 1. doi:10.1016/j.newar.2017.07.001
- Liu, Y., Sun, H., Xu, D., et al. 2025, Nature Astronomy, 9, 564. doi:10.1038/s41550-024-02449-8

- Lyons, N., O'Brien, P. T., Zhang, B., et al. 2010, MNRAS, 402, 2, 705. doi:10.1111/j.1365-2966.2009.15538.x
- Lü, H.-J. & Zhang, B. 2014, ApJ, 785, 1, 74. doi:10.1088/0004-637X/785/1/74
- Lü, H.-J., Yuan, H.-Y., Yi, T.-F., et al. 2022, ApJL, 931, 2, L23. doi:10.3847/2041-8213/ac6e3a
- Lü, H.-J., Zhang, B., Liang, E.-W., et al. 2014, MNRAS, 442, 3, 1922. doi:10.1093/mnras/stu982
- Lü, H.-J., Lan, L., Zhang, B., et al. 2018a, ApJ, 862, 2, 130. doi:10.3847/1538-4357/aacd03
- Lü, H.-J., Liang, E.-W., Zhang, B.-B., et al. 2010, ApJ, 725, 2, 1965. doi:10.1088/0004-637X/725/2/1965
- Lü, H.-J., Zou, L., Lan, L., et al. 2018b, MNRAS, 480, 4, 4402. doi:10.1093/mnras/sty2176
- Ma, Q., Maio, U., Ciardi, B., et al. 2015, MNRAS, 449, 3, 3006. doi:10.1093/mnras/stv477
- Maio, U., Salvaterra, R., Moscardini, L., et al. 2012, MNRAS, 426, 3, 2078. doi:10.1111/j.1365-2966.2012.21850.x
- Malesani, D., Tagliaferri, G., Chincarini, G., et al. 2004,  ${\it ApJL,\,609,\,1,\,L5.\,doi:10.1086/422684}$
- Malesani, D. B. & Izzo, L. 2025, GCN, 38930, 1.
- Malesani, D. B., Saccardi, A., Vergani, S. D., et al. 2025, GCN, 38934, 1.
- Matsumoto, T., Harikane, Y., Maeda, K., et al. 2024, ApJL, 976, 1, L16. doi:10.3847/2041-8213/ad8ce0
- Metzger, B. D., Giannios, D., Thompson, T. A., et al. 2011, MNRAS, 413, 3, 2031.
- doi:10.1111/j.1365-2966.2011.18280.x
- Metzger, M. R., Djorgovski, S. G., Kulkarni, S. R., et al. 1997, Nature, 387, 6636, 878. doi:10.1038/43132
- Modjaz, M., Stanek, K. Z., Garnavich, P. M., et al. 2006, ApJL, 645, 1, L21. doi:10.1086/505906
- $\label{eq:Nakar} \begin{array}{lll} {\rm Nakar,\ E.\ \&\ Piran,\ T.\ 2017,\ ApJ,\ 834,\ 1,\ 28.} \\ {\rm doi:}10.3847/1538\text{-}4357/834/1/28} \end{array}$
- Nousek, J. A., Kouveliotou, C., Grupe, D., et al. 2006, ApJ, 642, 1, 389. doi:10.1086/500724
- Paczynski, B. 1986, ApJL, 308, L43. doi:10.1086/184740 Paczynski, B. 1991, AcA, 41, 257.
- Paynter, J., Webster, R., & Thrane, E. 2021, Nature Astronomy, 5, 560. doi:10.1038/s41550-021-01307-1
- Pérez-Fournon, I. & Poidevin, F. 2025, GCN, 38943, 1.
- Perna, R., Armitage, P. J., & Zhang, B. 2006, ApJL, 636, 1, L29. doi:10.1086/499775
- Petrosian, V. & Dainotti, M. G. 2024, ApJL, 963, 1, L12. doi:10.3847/2041-8213/ad2763
- Pian, E., Mazzali, P. A., Masetti, N., et al. 2006, Nature, 442, 7106, 1011. doi:10.1038/nature05082
- Proga, D. & Zhang, B. 2006, MNRAS, 370, L61. doi:10.1111/j.1745-3933.2006.00189.x

- Rastinejad, J. C., Gompertz, B. P., Levan, A. J., et al. 2022, Nature, 612, 7939, 223. doi:10.1038/s41586-022-05390-w
- Robertson, B. E. & Ellis, R. S. 2012, ApJ, 744, 2, 95. doi:10.1088/0004-637X/744/2/95
- Rowlinson, A., O'Brien, P. T., Metzger, B. D., et al. 2013, MNRAS, 430, 2, 1061. doi:10.1093/mnras/sts683
- Rowlinson, A., Gompertz, B. P., Dainotti, M., et al. 2014, MNRAS, 443, 2, 1779. doi:10.1093/mnras/stu1277
- Salvaterra, R., Maio, U., Ciardi, B., et al. 2013, MNRAS, 429, 3, 2718. doi:10.1093/mnras/sts541
- Salvaterra, R., Della Valle, M., Campana, S., et al. 2009, Nature, 461, 7268, 1258. doi:10.1038/nature08445
- Sarin, N., Hübner, M., Omand, C. M. B., et al. 2024, MNRAS, 531, 1, 1203. doi:10.1093/mnras/stae1238
- Savchenko, V., Ferrigno, C., Kuulkers, E., et al. 2017, ApJL, 848, 2, L15. doi:10.3847/2041-8213/aa8f94
- Scargle, J. D. 1998, ApJ, 504, 1, 405. doi:10.1086/306064
- Schneider, B., Le Floc'h, E., Arabsalmani, M., et al. 2022, A&A, 666, A14. doi:10.1051/0004-6361/202243367
- Shan, Y., Liu, X., Yang, X., et al. 2024, Research in Astronomy and Astrophysics, 24, 8, 085003. doi:10.1088/1674-4527/ad58a7
- Speagle, J. S. 2020, MNRAS, 493, 3, 3132. doi:10.1093/mnras/staa278
- Stanek, K. Z., Matheson, T., Garnavich, P. M., et al. 2003, ApJL, 591, 1, L17. doi:10.1086/376976
- Stratta, G., Dainotti, M. G., Dall'Osso, S., et al. 2018, ApJ, 869, 2, 155. doi:10.3847/1538-4357/aadd8f
- Sun, H., Wang, C.-W., Yang, J., et al. 2025, National Science Review, 12, 3, nwae401. doi:10.1093/nsr/nwae401
- Tanvir, N. R., Fox, D. B., Levan, A. J., et al. 2009, Nature, 461, 7268, 1254. doi:10.1038/nature08459
- Tian, X., Lü, H., Tan, W., et al. 2025, ApJ, 982, 1, 19. doi:10.3847/1538-4357/adb711
- Troja, E., Fryer, C. L., O'Connor, B., et al. 2022, Nature, 612, 7939, 228. doi:10.1038/s41586-022-05327-3
- Troja, E., Cusumano, G., O'Brien, P. T., et al. 2007, ApJ, 665, 1, 599. doi:10.1086/519450
- Uhm, Z. L. & Zhang, B. 2015, ApJ, 808, 1, 33. doi:10.1088/0004-637X/808/1/33
- Usov, V. V. 1992, Nature, 357, 6378, 472. doi:10.1038/357472a0
- Vergani, S. D., Salvaterra, R., Japelj, J., et al. 2015, A&A, 581, A102. doi:10.1051/0004-6361/201425013
- Virgili, F. J., Liang, E.-W., & Zhang, B. 2009, MNRAS, 392, 1, 91. doi:10.1111/j.1365-2966.2008.14063.x
- Wang, F. Y., Bromm, V., Greif, T. H., et al. 2012, ApJ, 760, 1, 27. doi:10.1088/0004-637X/760/1/27
- Wang, X.-Y. & Mészáros, P. 2007, ApJ, 670, 2, 1247. doi:10.1086/522820

- Wang, Y., Moradi, R., & Li, L. 2024, ApJ, 974, 1, 89. doi:10.3847/1538-4357/ad6845
- $Woosley, S.\ E.\ \&\ Bloom,\ J.\ S.\ 2006,\ ARA\&A,\ 44,\ 1,\ 507.$  doi:10.1146/annurev.astro.43.072103.150558
- Yang, B., Jin, Z.-P., Li, X., et al. 2015, Nature Communications, 6, 7323. doi:10.1038/ncomms8323
- Yang, J., Ai, S., Zhang, B.-B., et al. 2022, Nature, 612, 7939, 232. doi:10.1038/s41586-022-05403-8
- Yang, Y.-H., Troja, E., O'Connor, B., et al. 2024, Nature, 626, 8000, 742. doi:10.1038/s41586-023-06979-5
- Yang, X., Lü, H.-J., Yuan, H.-Y., et al. 2021, ApJL, 921, L29. doi:10.3847/2041-8213/ac2f39
- Yu, W.-Y., Lü, H.-J., Yang, X., et al. 2024, ApJ, 962, 1, 6. doi:10.3847/1538-4357/ad1756

- Zhang, B.-B., Zhang, B., Sun, H., et al. 2018, Nature Communications, 9, 447. doi:10.1038/s41467-018-02847-3
- Zhang, B. 2006, Nature, 444, 7122, 1010. doi:10.1038/4441010a
- Zhang, B., Liang, E., Page, K. L., et al. 2007, ApJ, 655, 2, 989. doi:10.1086/510110
- Zhang, B. & Mészáros, P. 2001, ApJL, 552, 1, L35. doi:10.1086/320255
- Zhang, B., Zhang, B.-B., Virgili, F. J., et al. 2009, ApJ, 703, 2, 1696. doi:10.1088/0004-637X/703/2/1696
- Zhang, B. 2025, Journal of High Energy Astrophysics, 45, 325. doi:10.1016/j.jheap.2024.12.013

 $\textbf{Table 1.} \ \ \textbf{The Fitting Results of Time-resolved Spectra with CPL model for GRB\ 250114A}$ 

Time interval (s)	-10-20	20-50	112-137	210-232	232-253	253-282	282-320
Γ	$-0.02 \pm 0.73$	$0.30 \pm 0.62$	$1.23\pm0.02$	$0.96 \pm 0.17$	$1.06\pm0.06$	$0.72 \pm 0.03$	$0.91 \pm 0.03$
$E_{\rm p}~({\rm keV})$	$23 \pm 10$	$52 \pm 31$	$55 \pm 16$	$7 \pm 4$	$28 \pm 13$	$46 \pm 5$	$50 \pm 11$

 $\textbf{Table 2.} \ \ \text{The empirical Fitting Results of the X-ray Afterglow Light Curves with power-law} \ + \ \text{two smooth broken power-law models for GRB 250114A}$ 

	α	$egin{array}{c} t_b \ ( ext{s}) \end{array}$	$(\operatorname{erg} \operatorname{cm}^{-2} \operatorname{s}^{-1})$
Powe-law	$\alpha_1 = 4.22^{+0.19}_{-0.18}$	-	-
Flare	$\alpha_2 = -9.14^{+0.38}_{-0.38}$ $\alpha_3 = 7.52^{+0.15}_{-0.14}$	$t_{ m b,2}\sim 278$	$F_{\rm b,2} = (4.33 \pm 0.08) \times 10^{-9}$
Plateau	$\alpha_4 = 0.53^{+0.02}_{-0.03}$ $\alpha_5 = 1.70^{+0.38}_{-0.28}$	$t_{\rm b,3} = 15859^{+2531}_{-2343}$	$F_{\rm b,3} = (2.48 \pm 0.30) \times 10^{-12}$

Table 3. The Parameters of magnetar model fits and its inferred for GRB 250114A

Parameter	$A_1$	$\alpha_1$	$L_0  (10^{48}  \mathrm{erg  s^{-1}})$	$\tau$ (s)	n	$B_{\rm p} \left( \times 10^{15} \ {\rm G} \right)$	$P_0$ (ms)
Value	$117525_{-34038}^{+52577}$	$-3.22^{+0.10}_{-0.11}$	$2.78^{+0.46}_{-0.42}$	$2397^{+1057}_{-310}$	$2.44^{+0.55}_{-0.45}$	$13.24^{+1.73}_{-5.84}$	$14.31^{+0.93}_{-3.16}$

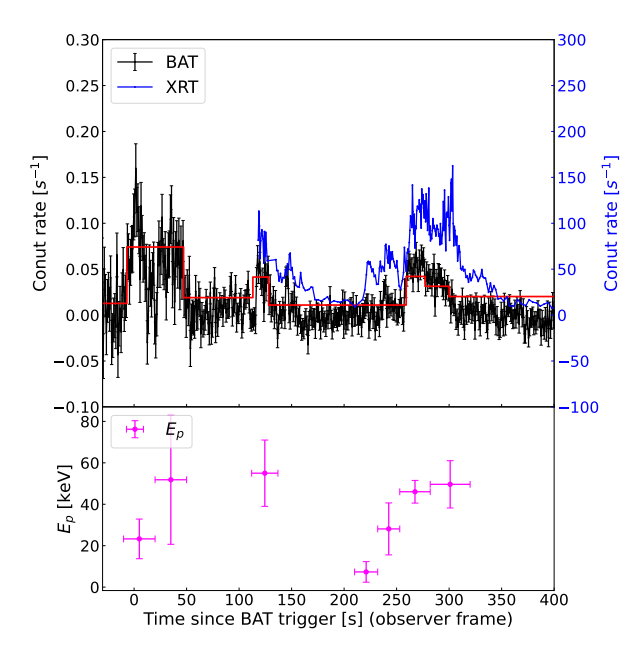


Figure 1. Light curves of prompt emission (black line in top panel) observed by BAT and X-ray emission (blue line in top panel), as well as  $E_p$  evolution (bottom panel) of GRB 250114A. The red step line is Bayesian block analysis for BAT light curve.

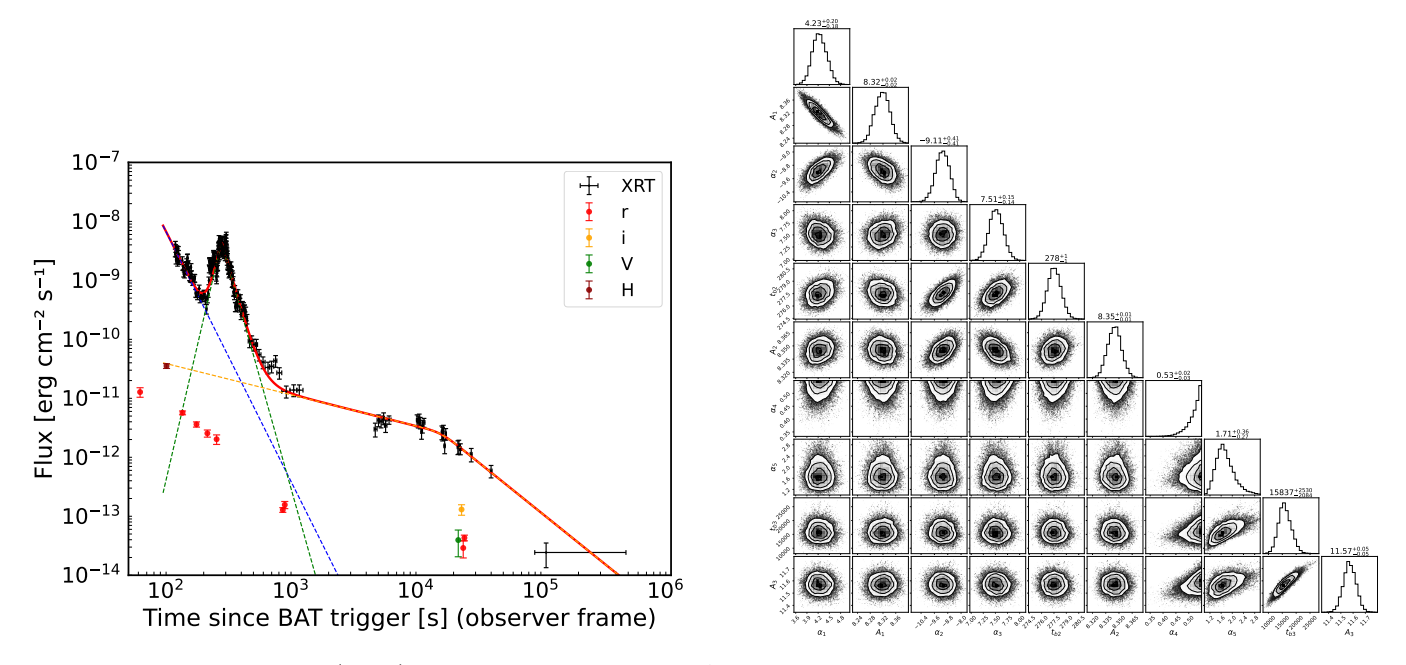


Figure 2. Left panel: XRT (black) light curve of GRB 250114A. The red solid line represents the total component fitting line. The blue, green, and orange dashed lines are the best fits for the power-law, flare and plateau, respectively. The red, yellow, green and darkred data points are multiband optical data collected from GCN reports. Right panel: corner plots and parameter constraints for the fitting parameters of the XRT light curve of GRB 250114A.

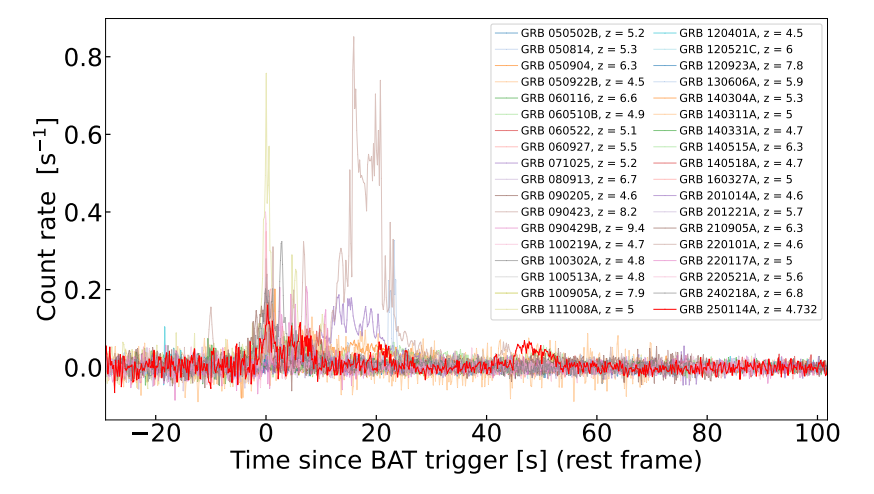


Figure 3. Comparison of GRB 250114A and Swift sample-GRBs with z>4.5 in prompt emission.

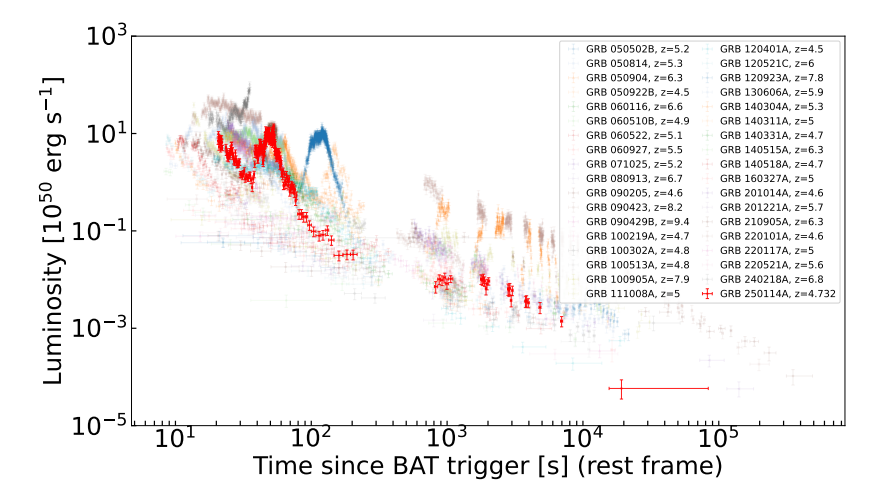
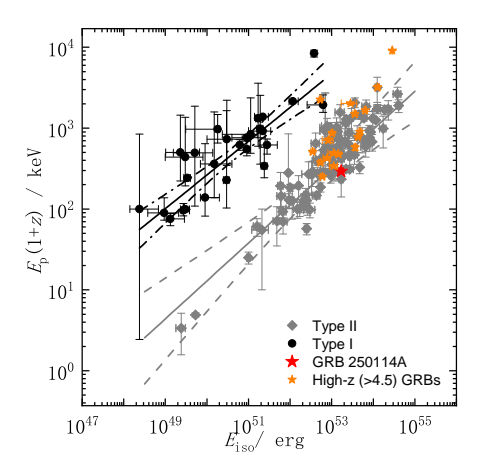


Figure 4. Comparison of GRB 250114A and Swift sample-GRBs with z>4.5 in X-ray afterglow.



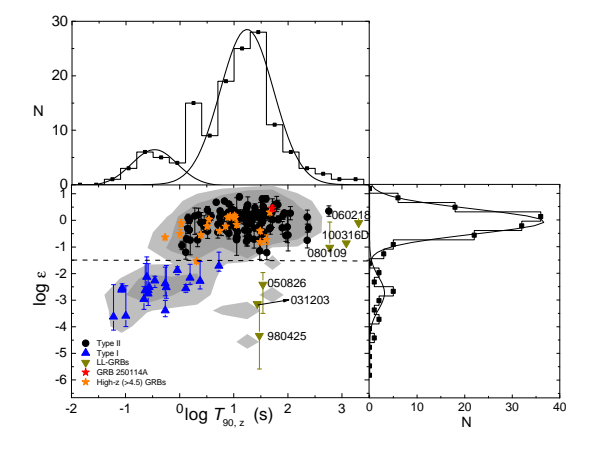


Figure 5. Left panel:  $E_{\rm p}$  and  $E_{\gamma,\rm iso}$  correlation diagram. Black points and gray diamonds correspond to Type I and Type II GRBs, respectively. The red star is GRB 250114A, and other data are taken from Zhang et al. (2009). Right panel: 1D and 2D distributions of GRB samples in  $T_{90} - \epsilon$  space. The dashed line indicates  $\epsilon = 0.03$ , and the data come from Lü et al. (2010)

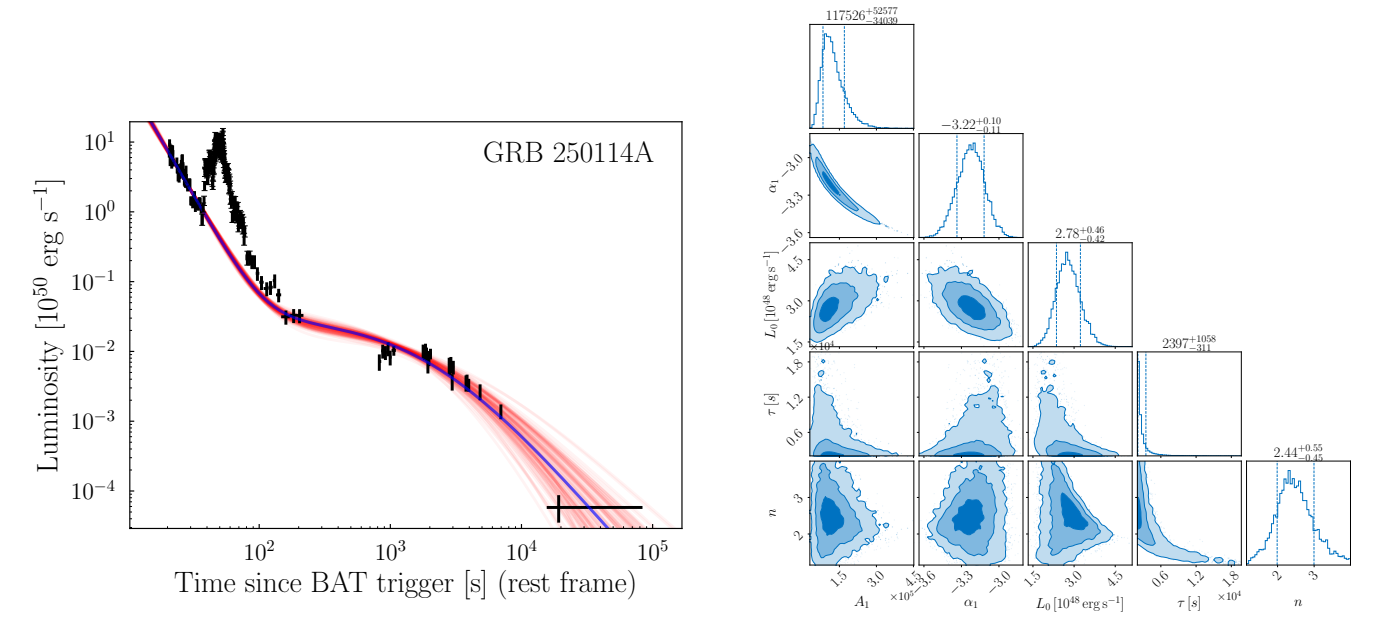


Figure 6. Left panel: X-ray light curve of GRB 250114A (black points) with magnetar model fits. The solid black line represents the maximum likelihood model, while the red lines represent 100 posterior samples, illustrating the uncertainty in the model fit. Right panel: 2D histograms and parameter constraints of the model fits for GRB 250114A. The 1D histograms show the distributions for each parameter. The dashed lines indicate the median and  $\pm 2\sigma$  uncertainty of the values.

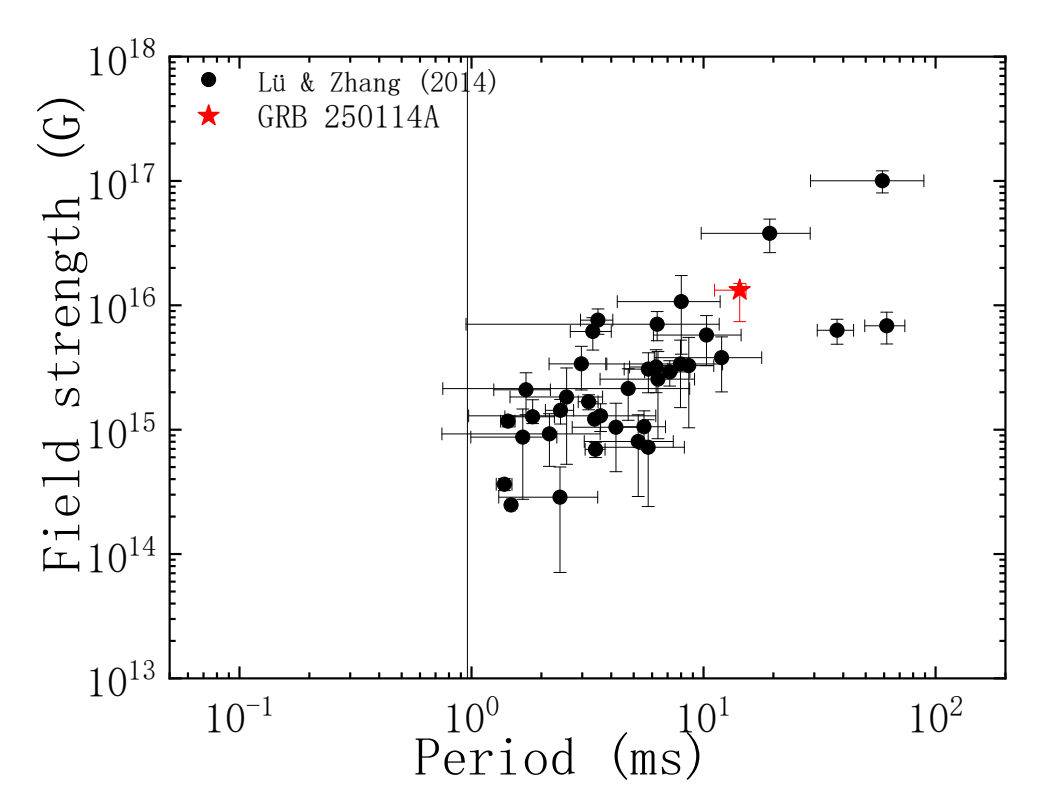


Figure 7. Inferred magnetar parameters of GRB 250114A, initial spin period  $P_0$  vs. surface polar cap magnetic field strength  $B_p$ . Other candidates for the magnetar cental engine are taken form Lü & Zhang (2014). The vertical solid line is the breakup spin period for a neutron star (Lattimer & Prakash 2004).